**Table 6.** Input parameters for example physical model of 177-341

 Stellar spectrum:
  $T_* = 39\,000\,\mathrm{K}$  

 (Simón-Díaz et al. 2006)
  $\log g = 4.1$ 
 $L_* = 2.04 \times 10^5\,L_\odot$  

 Ionizing flux at proplyd:
  $\Phi_{\mathrm{H}} = 1.58 \times 10^{13}\,\mathrm{cm}^{-2}\,\mathrm{s}^{-1}$  

 Ionization front radius:
  $r_0 = 1.91 \times 10^{15}\,\mathrm{cm}$  

 Gas-phase abundances:
 He 10.98, C 8.41, N 7.85, O 8.30,

  $(12 + \log_{10} z/\mathrm{H})$  Ne 7.56, S 6.98, Ar 6.26, Fe 5.65

 Dust composition:
 Standard Orion (Baldwin et al. 1991)

## 6.3 A physical model of 177-341

As an alternative to the purely empirical analysis presented in the previous sections, a different approach to analysing the emission spectrum of the proplyds is through the construction of physical models that combine a priori simulations of radiative transfer, hydrodynamics, and atomic physics in order to predict the density, temperature, and ionization structure of the proplyd flow. Such models have previously been applied to the ensemble properties of large numbers of proplyds (Johnstone, Hollenbach, & Bally 1998; Henney & Arthur 1998) and in detail to individual objects such as 177-341 (Henney & O'Dell 1999), LV2 (Henney et al. 2002), and LV1 (Graham et al. 2002). We have improved on these models in two significant ways. First, whereas published models have considered only emission from regions where hydrogen is fully ionized and the flow is supersonic, we now use a detailed analytic model of gas acceleration in the ionization front (Henney et al. 2005) to extend the treatment to cover partially ionized emission zones where the gas moves subsonically. Second, whereas published models used ad hoc fitting functions to the emissivity structure, specifically tailored to only the brightest emission lines, we now use the plasma microphysics code Cloudy (Ferland et al. 1998) to self-consistently calculate the full physical structure and emission spectrum of the proplyd flow.

The input parameters for the model (values given in Table 6) are the radius of the ionization front at the proplyd cusp (assumed hemispherical), the intensity and spectral shape of the illuminating stellar radiation, and the composition (gas-phase elemental mix and dust grain populations) of the proplyd material. For most of these parameters, we have taken values from the literature, whereas the gas-phase abundances and incident ionizing flux have been adjusted slightly in an attempt to reproduce the observed emission line intensities. The stellar spectrum is that determined for the ionizing star  $\theta^1$  Ori C by spectroscopic analysis (Simón-Díaz et al. 2006). The ionization front radius is the value determined by fitting to HST emission line images (Henney & O'Dell 1999), while the adopted ionizing flux at the proplyd position corresponds to a physical separation of the proplyd from the ionizing star of  $2.13 \times 10^{17}$  cm if there is no intervening absorption. Given the observed angular separation of 25.84" (Bally et al. 1998), and assuming a distance to the Orion Nebula of 440 pc (O'Dell & Henney 2008, Appendix A), the projected separation is  $1.70 \times 10^{17}$  cm, implying an inclination angle of  $\simeq 55^{\circ}$ . The diffuse radiation field and the proplyd tail are ignored in this model, since the observational aperture (§ 2.2) only covers the head of the proplyd.

The basic structure of the model is that the radiation arrives the outer zones of the proplyd. These zones are at low gas density  $(1\times10^3~{\rm cm}^{-3})$  and consequently have a high ionization parameter. As one go inside the proplyd (less radius), the gas density and temperature increase. Approaching the ionization front the temperature reach a maximum of  $\simeq 11\,000~{\rm K}$ . In the ionization front itself, the temperature drops while the electron density climbs to a peak of

about  $3 \times 10^5$  cm<sup>-3</sup> and then also falls. This is equivalent to say that each radius within the proplyd have a particular combination of temperature and density.

Figures 10 and 11 show preliminary results of the emission line spectrum of such a model applied to 177-341. Figure 10 (a) shows the emission estructure of [S II] 6731 Å (red), [N II] 6584 Å (green), and [O III] 5007 Å (blue). The outer zones of the model at low density are highly ionized, emitting principally in [O III], as seen in the blue horizontal branch at  $\simeq 9700 \,\mathrm{K}$  in the upper left part of the figure. As one approaches the proplyd ionization front (direction of increasing density), the [N II] and then [S II] emission become relatively stronger (color changes to yellow) and the temperature increases, reaching a maximum of  $\simeq 11\,000\,\mathrm{K}$ . In the ionization front itself, where the recombination gas happends, the [S II] emission comes to dominate over [NII], giving rise to the orange-red branch that curves down and to the left. Figure 10 (b) shows the negative-colored of the same data as in a overlayed with the observational diagnostic curves from Fig. 7a ([S II] in red, [N II] in green, [O III] in blue). The white star shows the solution for  $n_e$ ,  $T_e$  obtained in § 4.2. under the assumption that the emission in all three ions is co-extensive at a single density and temperature. This solution lies well outside the locus of densities and temperatures seen in the model, even though the model does reproduce the observed line ratios. Instead, the model satisfies the constraints of the three diagnostic curves separately in three different regions, which are indicated schematically by the colored stars. Note, however that even within the emission region of each ion there is considerable variation in the physical conditions.

Figure 11 shows that the model generally reproduces very well the observed relative line intensities for 177-341 with the notable exception of the [O I] 6300 Å line, which has a predicted intensity of only half the observed value. This discrepancy may be explained if a significant fraction of the observed [O I] emission comes from dissociation of OH at the surface of the proplyd's circumstellar disk (Storzer & Hollenbach 1998), which is not included in our model. The only other disagreement is with the [S III] 6312 Å line, which is roughly 25% too high in the model (roughly 1.5 times the observational uncertainty). This may be an indication that the details of the stellar spectrum around 23 eV are not correctly modeled, although the disagreement is only marginal.

Given that the stellar spectrum is very well constrained, the only way to vary the model temperature by a significant amount is by changing the gas-phase metal abundances and thus the gas cooling rate. In particular, the temperature in the highly ionized outer regions of the proplyd is very sensitive to the oxygen abundance since the [O III] 5007 Å line is the major coolant there. In order to reproduce the observed line intensities (particularly the [O III] 4363 Å/5007 Å ratio), we find it necessary to reduce the oxygen abundance to less than 50% of the value that has been measured for the surrounding nebula (e.g., Esteban et al. 2004), which leads to a temperature of around 9500 K in the [O III] emission zone. Using the standard Orion gas-phase abundances gives temperatures of about 8500 K for the same zone and predicts  $[O III]/H\beta$  ratios that are considerably higher than observed for the nebular 5007 Å and 4959 Å lines, but lower than observed for the auroral 4363 Å line. Using the even higher abundances derived by Tsamis et al. (2011) for the proplyd LV2 implies temperatures as low as 7700 K and exacerbates the disagreement with the observations still further. For comparison, both varying the stellar effective temperature by ±1000 K (the uncertainty in the analysis of Simón-Díaz et al. 2006) or varying the ionizing flux by a factor of two (corresponding to the uncertainty in the inclination angle of the proplyd) only change the gas temperature by < 200 K, while varying the stellar atmosphere

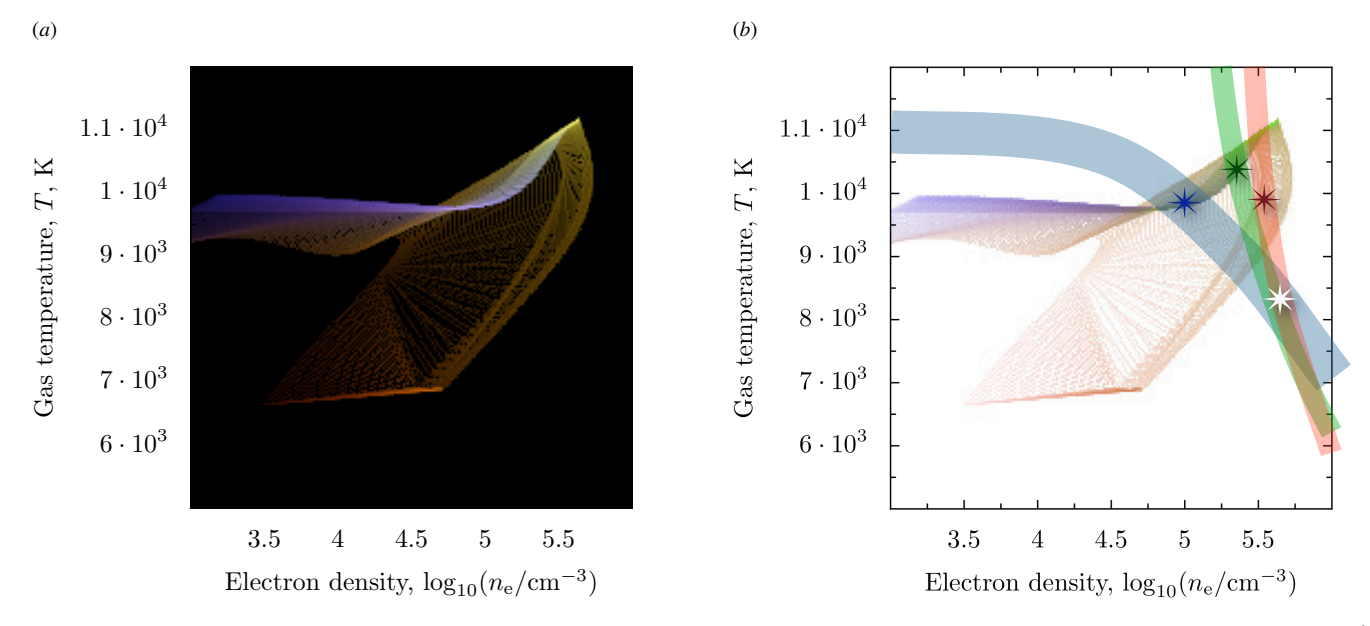


**Figure 10.** Emission structure in the  $n_e$ – $T_e$  plane for the example physical model of 177-341. (*a*) Positive-colored image of the three emission lines: [S II] 6731 Å (red), [N II] 6584 Å (green), and [O III] 5007 Å (blue), with brightness proportional to the fraction of the model luminosity in each line. (*b*) Negative-colored image of the same data as in *a* overlayed with the observational diagnostic curves from Fig. 7*a* ([S II] in red, [N II] in green, [O III] in blue).

model between WMBasic (Pauldrach et al. 2001) and TLUSTY (Lanz & Hubeny 2003) produces a slightly larger change of  $\simeq 400$  K.

Despite the promising success of the model in reproducing the observed line intensities, further work is necessary before a definitive statement can be made about the gas-phase abundances in the proplyd. The lack of observations of [OII] lines, together with the uncertain nature of the [O<sub>I</sub>] emission (see above) means that the oxygen abundance hinges on observations of a single ion stage. It is vital to test the model against other proplyds, particularly those such as LV2 (Tsamis et al. 2011; Tsamis & Walsh 2011) where the [OII] 3726, 3729 Å doublet is observed. At the same time, the models need to be simultaneously constrained not just by the line ratios, but also by sub-arcsecond HST imaging (Bally et al. 1998; O'Dell 1998) and velocity profiles from high-resolution spectroscopy (Henney & O'Dell 1999; Shuping et al. 2003). It is also necessary to examine in greater detail the potential influence of internal extinction within the proplyd. This depends on the properties of the dust that is entrained in the photoevaporation flow, which can be constrained by comparison with observations of thermal midinfrared emission (García-Arredondo et al. 2001; Smith et al. 2005; Robberto et al. 2005; Shuping et al. 2006).

## ACKNOWLEDGEMENTS

WJH and NFF acknowledge financial support from DGAPA-UNAM through project PAPIIT IN102012 and from a postdoctoral fellowship to NFF.

## References

Baldwin J. A., Ferland G. J., Martin P. G., Corbin M. R., Cota S. A., Peterson B. M., Slettebak A., 1991, ApJ, 374, 580
Bally J., Sutherland R. S., Devine D., Johnstone D., 1998, AJ, 116, 293

Esteban C., Peimbert M., García-Rojas J., Ruiz M. T., Peimbert A., Rodríguez M., 2004, MNRAS, 355, 229

Ferland G. J., Korista K. T., Verner D. A., Ferguson J. W., Kingdon J. B., Verner E. M., 1998, PASP, 110, 761

García-Arredondo F., Henney W. J., Arthur S. J., 2001, ApJ, 561, 830

Graham M. F., Meaburn J., Garrington S. T., O'Brien T. J., Henney W. J., O'Dell C. R., 2002, ApJ, 570, 222

Henney W. J., Arthur S. J., 1998, AJ, 116, 322

Henney W. J., Arthur S. J., Williams R. J. R., Ferland G. J., 2005, ApJ, 621, 328

Henney W. J., O'Dell C. R., 1999, AJ, 118, 2350

Henney W. J., O'Dell C. R., Meaburn J., Garrington S. T., López J. A., 2002, ApJ, 566, 315

Johnstone D., Hollenbach D., Bally J., 1998, ApJ, 499, 758

Lanz T., Hubeny I., 2003, ApJS, 146, 417

O'Dell C. R., 1998, AJ, 115, 263

O'Dell C. R., Henney W. J., 2008, AJ, 136, 1566

Pauldrach A. W. A., Hoffmann T. L., Lennon M., 2001, A&A, 375, 161

Robberto M. et al., 2005, AJ, 129, 1534

Shuping R. Y., Kassis M., Morris M., Smith N., Bally J., 2006, ApJ, 644, L71

Shuping R. Y., Patience J., Bally J., Morris M., Larkin J. E., Macintosh B. A., 2003, in Society of Photo-Optical Instrumentation Engineers (SPIE) Conference Series, Vol. 4834, Society of Photo-Optical Instrumentation Engineers (SPIE) Conference Series, P. Guhathakurta, ed., pp. 364–374

Simón-Díaz S., Herrero A., Esteban C., Najarro F., 2006, A&A, 448, 351

Smith N., Bally J., Shuping R. Y., Morris M., Kassis M., 2005, AJ, 130, 1763

Storzer H., Hollenbach D., 1998, ApJ, 502, L71

Tsamis Y. G., Walsh J. R., 2011, MNRAS, 417, 2072

Tsamis Y. G., Walsh J. R., Vílchez J. M., Péquignot D., 2011, MNRAS, 412, 1367

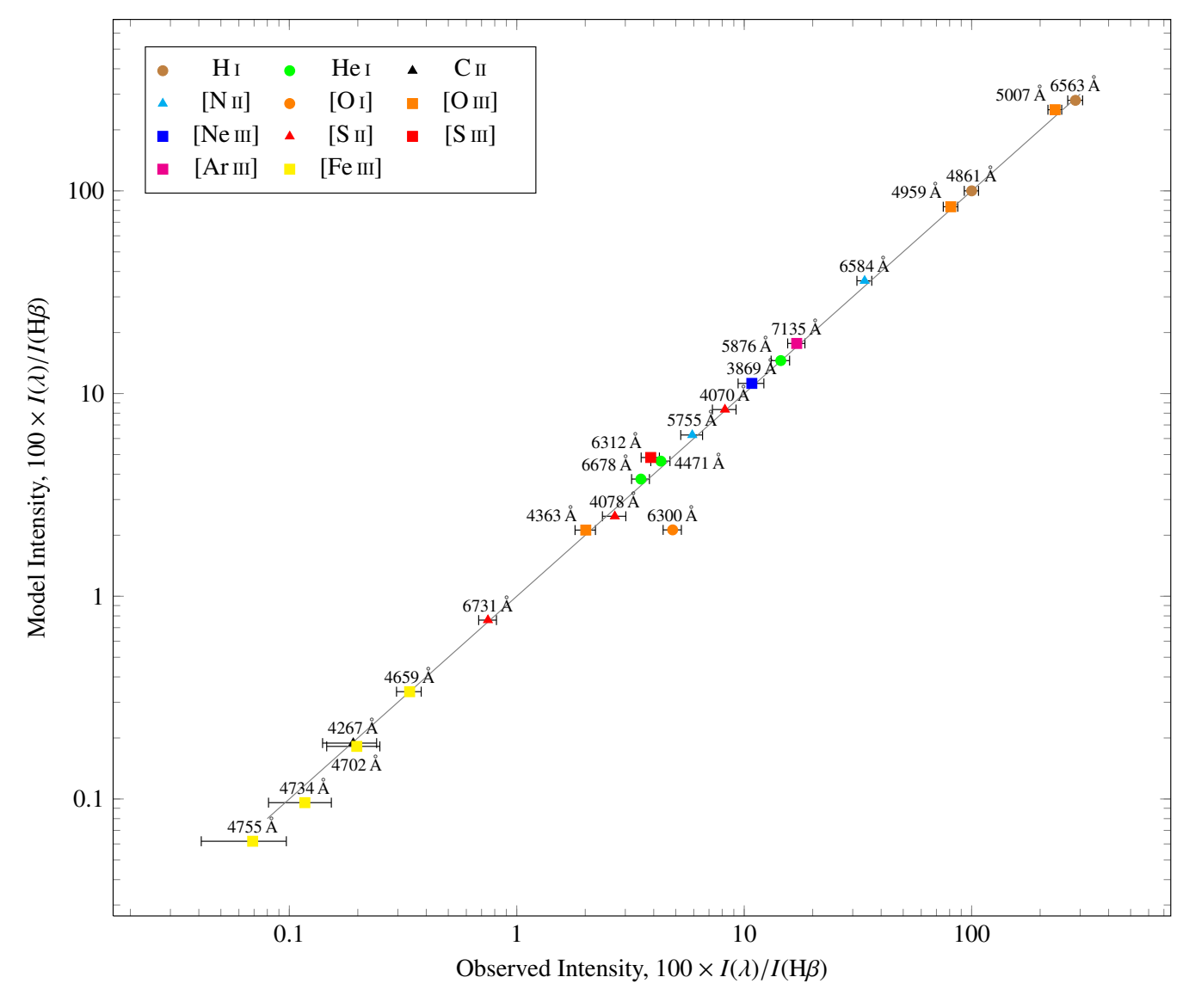


**Figure 11.** Comparison of model and observed line intensities for the proplyd 177-341. The model parameters are those given in Table 6 and the emission structure of the model is discussed in Fig. 10. Observed intensities correspond to the  $c(H\beta) = 0$  background-subtracted values given in column 4 of Table 2.